

# Statistical Approach for Fast Impairment-Aware Provisioning in Dynamic All-Optical Networks

L. Velasco, A. Jirattigalachote, M. Ruiz, P. Monti, L. Wosinska, and G. Junyent

**Abstract**—Physical layer impairments (PLIs) need to be considered in the routing and wavelength assignment (RWA) process of all-optical networks to ensure the provisioning of good quality optical connections (i.e., *lightpaths*). A convenient way to model the impact of PLIs on the signal quality is to use the so-called *Q*-factor. In a dynamic provisioning environment, impairment-aware RWA (IA-RWA) algorithms include *Q*-factor evaluation in their on-line decisions on whether to accept a connection request or not. The *Q*-factor can be computed in either an *approximated* or an *exact* way. IA-RWA algorithms using an approximated *Q*-factor estimation (i.e., worst case) can be very fast and allow for a short setup delay. However, connection request blocking can be unnecessarily high because of the worst-case assumption for the *Q*-factor parameters. In contrast, an exact *Q*-factor computation results in a better blocking performance at the expense of a longer setup delay, mainly due to the time spent for the *Q*-factor computation itself. Moreover, an exact *Q*-factor approach requires extensions of the generalized multi-protocol label switching suite. To overcome these problems, we propose a statistical approach for fast impairment-aware RWA (SAFIR) computation. The evaluation results reveal that SAFIR improves the blocking probability performance compared to the worst-case scenario without adding extra computational complexity and, consequently, without increasing the connection setup delay.

**Index Terms**—All-optical networks; Cross-phase modulation (XPM); Impairment-aware RWA.

## I. INTRODUCTION

The rapidly increasing traffic demand in communication networks requires further improvement of spectral efficiency in transparent dense wavelength division multiplexing (DWDM) networks where the signal is transmitted from source to destination through all-optical channels called lightpaths. With the absence of optical-to-electrical-to-optical (O/E/O) conversion at intermediate nodes, the optical signal might be degraded due to physical layer impairments (PLIs) induced by the transmission through optical fibers and components.

PLIs can be divided into *non-linear* and *linear* impairments. Non-linear impairments affect not only each wavelength channel individually, but also cause disturbance and interference among channels traversing the same fiber link. The most important non-linear effects are self-phase modulation (SPM), cross-phase modulation (XPM), and four-wave mixing (FWM). Non-linear impairments become in general apparent as the signal power increases in long-haul links. On the other hand, linear impairments do not depend on the signal power. The most important linear impairments are fiber attenuation, amplifier spontaneous emission (ASE) noise, chromatic dispersion (CD) (or group velocity dispersion (GVD)), and polarization mode dispersion (PMD). Linear and non-linear PLIs of a lightpath can be quantified by using the quality factor *Q* [1].

To provide good quality lightpaths, PLI information needs to be taken into account while solving the routing and wavelength assignment (RWA) problem. RWA consists in finding a physical route and in assigning a wavelength to a given connection request. The incorporation of PLI information into the RWA problem for transparent optical networks has recently received a lot of attention, resulting in the development of a number of impairment-aware RWA (IA-RWA) algorithms [1–10]. IA-RWA algorithms can be used either in the network planning phase, when the set of connection requests is known in advance (off-line algorithms) [2], or in the dynamic lightpath provisioning upon arrival of connection requests (dynamic algorithms). In dynamic IA-RWA algorithms, the *Q*-factor of candidate lightpaths is computed during the lightpath setup process, and only those lightpaths with a *Q*-factor above a pre-defined threshold are established. Two main approaches for dynamic IA-RWA can be considered, i.e., *centralized* and *distributed*. A distributed approach offers a shorter setup delay than a centralized one, but at the expense of a higher blocking probability [3,4]. In this paper, we focus on dynamic IA-RWA algorithm to be used in the distributed control plane of automatically switched optical networks (ASONs) [11].

When non-linear impairments are considered for RWA computation at each controller node of a distributed control plane, the information of the current network state (i.e., which wavelength channels are used on the fiber links) is needed for calculating the *Q*-factor of each wavelength that is end-to-end available for every candidate route. This translates into the need for standardized extensions of the generalized multi-protocol label switching (GMPLS) protocol set [12] in order to provide the necessary information for a distributed and accurate IA-RWA computation.

Manuscript received July 20, 2011; revised January 3, 2012; accepted January 6, 2012; published January 30, 2012 (Doc. ID 151414).

L. Velasco (e-mail: lvelasco@ac.upc.edu), M. Ruiz, and G. Junyent are with the Advanced Broadband Communications Center (CCABA), Universitat Politècnica de Catalunya (UPC), Barcelona, Spain.

A. Jirattigalachote, P. Monti, and L. Wosinska are with the School of Information and Communication Technology (ICT), Royal Institute of Technology (KTH), Kista, Sweden.

Digital Object Identifier 10.1364/JOCN.4.000130

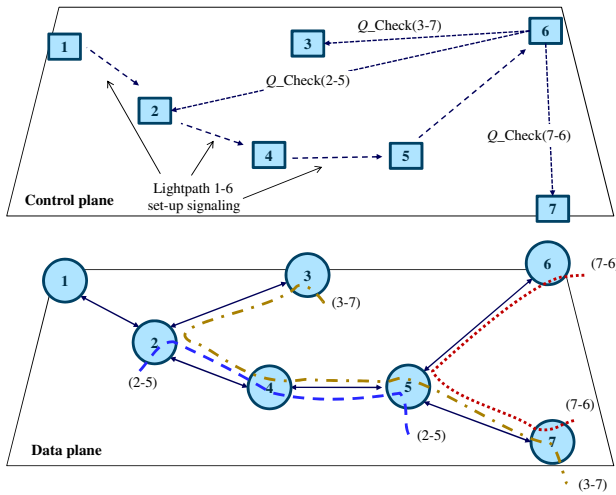


Fig. 1. (Color online) Example of  $Q$ -factor re-computation ( $Q\_Check$ ) when a new lightpath is established in the network.

Extensions of the signaling protocol to collect information about the already-established lightpaths along the route of a new lightpath during its setup signaling phase are studied in [9,10]. Before establishing a new lightpath, the  $Q$ -factor of the already-established lightpaths sharing common links with the new one is re-computed to ensure that their signal qualities will not be degraded below a specified threshold if the new lightpath were to be established. Figure 1 shows an example of  $Q$ -factor re-computation after the arrival of a new connection request. Assume that three lightpaths (2–5, 3–7, and 7–6) are already established in the optical data plane. When a new request for a connection between nodes 1 and 6 arrives, the RWA algorithm at the source node in the control plane (controller 1) computes a route through the links 1–2, 2–4, 4–5, and 5–6. Note that the new lightpath shares some of those links with the already-established lightpaths, i.e., lightpaths 2–5, 3–7, and 7–6. Since establishing a new lightpath might affect the signal quality of the already-established ones, the information about these lightpaths needs to be collected during the new connection setup signaling. At the destination node (controller 6), the  $Q$ -factor of both the new and all affected lightpaths is computed, requiring a new protocol to request  $Q$ -factor re-computation to be standardized. Moreover, if any of these lightpaths have a  $Q$ -factor lower than a pre-defined threshold, an error needs to be generated followed by a new route re-computation at the source node, and a new signaling process is started. As a consequence, all these processes, i.e., collecting lightpath information and  $Q$ -factor re-computation, not only add complexity and control overhead, but also increase the lightpath setup delay.

Several approaches have been proposed to prevent the prohibitively high control overhead of the (accurate) distributed approach while reducing the lightpath setup delay. The authors of [8] consider impairments as fixed penalties for each link assuming a fully loaded system, referred to as the worst-case approach. Advantages of this approach are (i) very short lightpath setup time (impairments of each link can be pre-computed), and (ii) GMPLS protocol extensions are not

needed. However, the blocking probability obtained using this approach might be unnecessarily high.

With respect to the  $Q$ -factor, XPM is the dominant non-linear impairment, the value of the XPM variance being several times greater than that of FWM [13]. For example, for a path with a  $Q$ -factor of 7.3 (bit error rate (BER)  $\approx 1.44e-13$ ), the values of the variance of XPM and FWM are  $1.58e-4$  and  $5.66e-6$ , respectively. Thus, in this case, the XPM variance is more than 27 times greater than the FWM variance. Therefore, several works present not only analytical models to compute the XPM, but also ways to accelerate that computation. The authors in [14] studied the spectral characteristics of XPM in multi-span optical systems and found that per span dispersion compensation is the most effective way to minimize the effect of XPM. In [15], a generalized model of the XPM degradation in fiber links consisting of multiple fiber segments with different characteristics and optical amplifiers is presented. Although this original model was subsequently simplified in other works (e.g., [16]),  $Q$ -factor computation times were still of the order of seconds and thus impractical when used in the control plane, even using ad hoc hardware-accelerated computation [17]. Other approaches to minimizing setup times in an on-line provisioning paradigm resort to the use of guard bands, i.e., leaving unused wavelength channels between lightpaths in order to reduce the effect of XPM [18].

To overcome the deficiencies of the existing IA-RWA approaches, this paper proposes (i) a statistical model for fast and accurate estimation of XPM noise-like variance which allows one to obtain the  $Q$ -factor of a given lightpath with computation times several orders of magnitude lower without employing additional hardware, and (ii) a novel probabilistic approach, called SAFIR (statistical approach for fast impairment-aware RWA), which uses the proposed statistical XPM model and wavelength channel usage values (obtained by network characterization) to calculate the  $Q$ -factor of a lightpath without requiring  $Q$ -factor re-computation of already-established lightpaths or GMPLS extensions. Keeping in mind the lesson learnt from the guard band concept, our approach defines a parameter called the channel-interference negligible distance ( $\eta$ ), which determines the range of neighboring wavelength channels that significantly interfere with the one under study. In contrast with guard bands, channels in the  $\eta$  range with respect to a given reference channel can be used as long as they can provide a  $Q$  value better than a given  $Q$  threshold. Simulation results show that SAFIR drastically improves the network efficiency, achieving performance similar to that of the accurate distributed approach, with a shorter computation time.

The remainder of this paper is organized as follows. Section II introduces the general impairments model and presents the proposed statistical XPM model. Section III describes the SAFIR approach based on network characterization used to apply probability to the IA-RWA process. The derived statistical XPM model and the probabilistic IA-RWA algorithm are subsequently applied to different reference network topologies in Section IV. Finally, Section V gives some concluding remarks.

## II. IMPAIRMENTS MODEL

This section first presents a description of how the  $Q$ -factor is computed, and then it describes in detail the proposed statistical model for an approximation of the XPM value.

### A. $Q$ -factor Computation

As stated above, the effect of both linear and non-linear PLIs can be quantified by using the quality factor  $Q$ .

In [1] the authors present a  $Q$ -factor estimation model that includes the effects of ASE noise, the combined SPM/GVD and optical filtering effects, XPM, and FWM. Here, we extend that model to include also the power penalty due to PMD. ASE, FWM, and XPM are calculated assuming that they follow a Gaussian distribution. The combined SPM/GVD and optical filtering effects are quantified through an eye closure metric calculated on the most degraded bit pattern. The power penalty due to PMD is calculated based on the length of a lightpath, the bit rate, and the fiber PMD parameter. Based on these assumptions, in this paper, the  $Q$ -factor of a lightpath is calculated according to the following equation, where  $P_{\text{transmitter}}$  is the transmitted signal power,  $pen_{\text{eye}}$  is the relative eye closure penalty attributed to SPM/GVD and optical filtering effects,  $pen_{\text{PMD}}$  is the power penalty due to PMD, and  $\sigma_{\text{ASE}}^2$ ,  $\sigma_{\text{XPM}}^2$ , and  $\sigma_{\text{FWM}}^2$  are the electrical variance of ASE noise, XPM, and FWM, respectively. A detailed analytical expression of each term in Eq. (1) can be found in [1].

$$Q = \frac{pen_{\text{eye}} \cdot P_{\text{transmitter}}}{pen_{\text{PMD}} \cdot \sqrt{\sigma_{\text{ASE}}^2 + \sigma_{\text{XPM}}^2 + \sigma_{\text{FWM}}^2}}. \quad (1)$$

$pen_{\text{eye}}$ ,  $pen_{\text{PMD}}$ , and  $\sigma_{\text{ASE}}^2$  can be computed beforehand, since their values do not vary with the load of the network (i.e., the number of currently used wavelength channels). Nonetheless, the values of  $\sigma_{\text{XPM}}^2$  and  $\sigma_{\text{FWM}}^2$  vary with the load, and they need to be computed for every end-to-end unused wavelength of a candidate route. We computed the value of  $\sigma_{\text{XPM}}^2$  for several link distances and number of wavelengths scenarios on a dual-core-based computer with 4 Gbytes of RAM, and the computation time took 50 ms on average. As will be demonstrated, the lightpath setup process with a distributed control plane based on an IA-RWA algorithm would be of the order of seconds (which is in line with [17]). As explained in the previous section, the  $Q$ -factor of each candidate lightpath needs to be evaluated to choose the best performing lightpath and the  $Q$ -factor of each already-established lightpath needs to be re-computed to guarantee that the signal quality of already-established lightpaths is not affected after establishing a new one. This strategy is obviously impractical in the control plane of ASONs.

To overcome this deficiency, we propose next a statistical model for accurate and fast  $\sigma_{\text{XPM}}^2$  computation. Since  $\sigma_{\text{XPM}}^2$  is dominant over  $\sigma_{\text{FWM}}^2$ , the worst-case value of  $\sigma_{\text{FWM}}^2$  is assumed in this paper, and thus it can be computed in advance.

### B. Statistical XPM Model

Let  $G(N, E, W)$  represent a graph of an optical network, where  $N$  is the set of nodes,  $E$  is the set of fiber links, and  $W$  is the set of wavelengths in ascending order of their respective frequencies. Every wavelength in  $W$  is assigned a wavelength channel labeled from 1 to  $|W|$ . Let  $\alpha(e)$  be the number of amplifiers along every link  $e \in E$ .  $\sigma_{\text{XPM}}^2(e, \lambda)$  represents the XPM noise variance on reference channel  $\lambda$  of the link  $e$ , which suffers from interference with every other wavelength channel of link  $e$  used.  $\sigma_{\text{XPM}}^2(e, \lambda, i)$  is the XPM noise variance on reference channel  $\lambda$  as a consequence of the interference with channel  $i$  of link  $e$ .

Aiming at empirically describing the relation between  $\sigma_{\text{XPM}}^2(e, \lambda)$  and  $\sigma_{\text{XPM}}^2(e, \lambda, i)$ , we developed a factorial experiment [19] consisting of thousands of XPM variance computations using the analytical model proposed in [16]. Each computation is characterized by a unique combination of experimental variables: the number of in-line amplifiers along a link, the number of wavelengths on a link, the reference channel, and the status of the other channels (i.e., busy or free). Note that, when the number of busy channels is equal to one, the  $\sigma_{\text{XPM}}^2(e, \lambda)$  value obtained matches a specific case of  $\sigma_{\text{XPM}}^2(e, \lambda, i)$ . The results obtained using statistical correlation are in perfect accordance with the following equation, deduced from [15,16], where  $\delta_i(e)$  is a binary variable which is equal to 1 if channel  $i$  is busy, and 0 otherwise.

$$\sigma_{\text{XPM}}^2(e, \lambda) = \sum_{\substack{i \in W \\ i \neq \lambda}} \delta_i(e) \cdot \sigma_{\text{XPM}}^2(e, \lambda, i). \quad (2)$$

In conclusion, each channel occupied by an active lightpath adds some interference to the XPM variance of the reference channel regardless of the status of the rest of the channels. Due to this additive behavior, it is possible to find an alternative model to calculate  $\sigma_{\text{XPM}}^2(e, \lambda)$  based on the modeling of  $\sigma_{\text{XPM}}^2(e, \lambda, i)$ . Note that the value of  $\sigma_{\text{XPM}}^2(e, \lambda, i)$  is computed using the equation presented in [1], where the effects of signal power, fiber effective area, fiber length, fiber attenuation, non-linear index coefficient, dispersion coefficient, and the walk-off parameter between the reference channel  $\lambda$  and channel  $i$  are taken into account.

The first and most straightforward approach (hereafter, the *full deterministic* approach) consists in pre-computing and storing the whole set of possible  $\sigma_{\text{XPM}}^2(e, \lambda, i)$  values.  $\sigma_{\text{XPM}}^2(e, \lambda, i)$  depends on three discrete variables (i.e.,  $\alpha(e)$ ,  $\lambda$ , and  $i$ ), which in turn create the set of finite and countable  $\sigma_{\text{XPM}}^2(e, \lambda, i)$  values. In fact, the size of this set is equal to  $|W| * (|W| - 1) * \max\text{Amp}$ , where  $\max\text{Amp} = \max(\alpha(e), e \in E)$ . This shows that the application of the full deterministic approach provides an alternative valid method to obtain exact XPM variance values in an on-line IA-RWA algorithm. However, the size of  $\sigma_{\text{XPM}}^2(e, \lambda, i)$  might become an issue in real networks. As will be shown in Section IV, the size of the  $\sigma_{\text{XPM}}^2(e, \lambda, i)$  set grows to the impractical value of 158,000 for 80 wavelengths.

To overcome the drawback of the full deterministic approach, we propose a two-step approach, referred to as the *restricted approximated* approach, to reduce the size of the set of possible values necessary to model  $\sigma_{\text{XPM}}^2(e, \lambda)$ . The restricted

approximated approach aims at (i) reducing the range of neighboring channels interfering with the reference channel, and (ii) obtaining polynomial models to describe  $\sigma_{\text{XPM}}^2(e, \lambda, i)$ .

To determine the range of neighboring channels that significantly interfere with a reference channel, we defined the *channel-interference negligible distance* ( $\eta$ ) as the parameter representing half of that range. Those channels at a distance greater than  $\eta$  from the reference channel are assumed to have negligible XPM interference on the reference channel. Equation (2) is modified to take into account the channel-interference negligible distance  $\eta$  as follows:

$$\sigma_{\text{XPM}}^2(e, \lambda) = \sum_{i=\max(1, \lambda-\eta)}^{\min(\lambda+\eta, |W|)} \delta_i(e) \cdot \sigma_{\text{XPM}}^2(e, \lambda, i) + \epsilon_{\text{link}}, \quad i \neq \lambda, \quad (3)$$

where  $\epsilon_{\text{link}}$  represents the error caused by ignoring the effect of the channels at a distance greater than  $\eta$  from  $\lambda$ . Equation (3) describes an intermediate step between the full deterministic and the restricted approximated models. Note that when  $\eta = |W| - 1$  the interference of every wavelength in the optical spectrum is considered, and the model in Eq. (3) is equal to the full deterministic model, i.e.,  $\epsilon_{\text{link}} = 0$ . By using the  $\sigma_{\text{XPM}}^2(e, \lambda)$  model shown in Eq. (3), the number of  $\sigma_{\text{XPM}}^2(e, \lambda, i)$  values to be computed in the worst case is reduced to  $2\eta * |W| * \text{maxAmp}$  (from  $\lambda - \eta$  to  $\lambda + \eta$ ), which, depending on the value of  $\eta$ , can be significantly smaller than the number of  $\sigma_{\text{XPM}}^2(e, \lambda, i)$  values needed in the full deterministic approach.

The second step of the restricted approximated approach is to find a model that is able to estimate the impact (i.e., interference) of each channel in the range  $[\lambda - \eta, \lambda + \eta]$  on the value of  $\sigma_{\text{XPM}}^2(e, \lambda)$ . Let  $s_{\text{XPM}}^2(e, \lambda, i)$  represent an approximate model of  $\sigma_{\text{XPM}}^2(e, \lambda, i)$ , such that  $\sigma_{\text{XPM}}^2(e, \lambda, i) \approx s_{\text{XPM}}^2(e, \lambda, i)$ . Keeping in mind that  $\sigma_{\text{XPM}}^2(e, \lambda, i)$ ,  $\lambda$ , and  $\alpha(e)$  are non-linearly related (as shown in Section IV), we propose a polynomial model of degree  $\gamma$  obtained by least squares interpolation [19] using  $\alpha(e)$  and  $\lambda$  as variables. The mathematical formulation of the polynomial is as follows:

$$s_{\text{XPM}}^2(e, \lambda, i) = \sum_{j \in [1, \gamma]} u_{ij} \cdot \lambda^j + \sum_{k \in [1, \gamma]} v_{ik} \cdot \alpha(e)^k + \sum_{j \in [1, \gamma]} \sum_{k \in [1, \gamma]} w_{ijk} \cdot \lambda^j \cdot \alpha(e)^k + b_i \pm \epsilon_{\text{pair}}, \quad (4)$$

where  $u$ ,  $v$ ,  $w$ , and  $b$  are the polynomial coefficients. The superscripts on the variables in Eq. (4) indicate the corresponding powers of the polynomial model. The number of coefficients of each  $\sigma_{\text{XPM}}^2(e, \lambda, i)$  model is  $(\gamma^2 + 2\gamma + 1)$ . Note that some of these coefficients could be zero. Moreover, for the sake of simplicity, we modeled every  $\sigma_{\text{XPM}}^2(e, \lambda, i)$  with the same parameter  $\gamma$  obtained by adjusting the error of each model to a given target. Thus, the total number of coefficients for the restricted approximated model (Eqs. (3) and (4)) is bounded to  $2\eta * (\gamma^2 + 2\gamma + 1)$ .

The next section presents a provisioning approach that uses this approximated PLI model, including the XPM model and the worst case for FWM.

### III. THE SAFIR APPROACH

This section presents SAFIR (Statistical Approach for Fast Impairment-aware RWA), a provisioning approach that bases its decisions on a probabilistic value of the  $Q$ -factor of the lightpaths. SAFIR consists of three phases. First, before the network is put into operation, the network is characterized by obtaining an *on-average* usage distribution of each channel for a given traffic matrix and intensity. In the second phase, i.e., during network operation, a probabilistic IA-RWA is used to accommodate dynamic connection requests. This probabilistic provisioning strategy takes advantage of the approximated impairments model described in the previous section. During this phase, the actual traffic distribution is monitored to detect deviations from the expected traffic distribution used in the first phase. When a significant discrepancy is detected, a network re-characterization phase (the third one) is triggered and the new channel usage data is disseminated to every node in the network. It is worth noting that the network design problem is out of the scope of this paper. In this regard, we assume that the traffic matrix used as a reference has been appropriately designed to cope with short-term traffic fluctuations, see, e.g., [20], giving as a result an expected traffic distribution and intensity.

#### A. Before Operation: Network Characterization

Before putting the network into operation, its potential behavior under the expected traffic distribution and intensity needs to be studied and characterized. The objective of this characterization process is to obtain an *on-average* usage distribution of each wavelength channel for the predicted traffic distribution and intensity. To this end, a number of simulations are run using a modified first-fit (FF) heuristic for the wavelength assignment, where the assignment order is modified to mimic the XPM behavior described in Section II with a given  $\eta$  value (i.e., the XPM noise variance is neglected for channels at a distance greater than the given  $\eta$ ), and without blocking any connection request due to a low value of the  $Q$ -factor.

The complete set of links of the given network is divided into several subsets as a function of their usage degree. We consider two subsets: subset 1, consisting of the most used links, i.e., mainly links with short physical distance; and subset 2, consisting of the least used links. Figure 2 shows an example of the cumulative distribution function of the usage probability obtained for three channels on links of subset 1 and subset 2 of the European Optical Network—Basic Topology, EON-BT (presented in Section IV). As shown in the figure, channels in subset 1 have a higher usage probability than the channels in subset 2. For instance, channel #9 is expected to be used with a probability of roughly 90% on links in subset 1 and with a probability of around 60% on links in subset 2. Note that a worst-case approach, which assumes that every channel is in use on every link [8], can be replaced with a probabilistic worst case using these probabilities. This already entails a significant improvement of the proposed probabilistic approach with respect to the worst-case one.

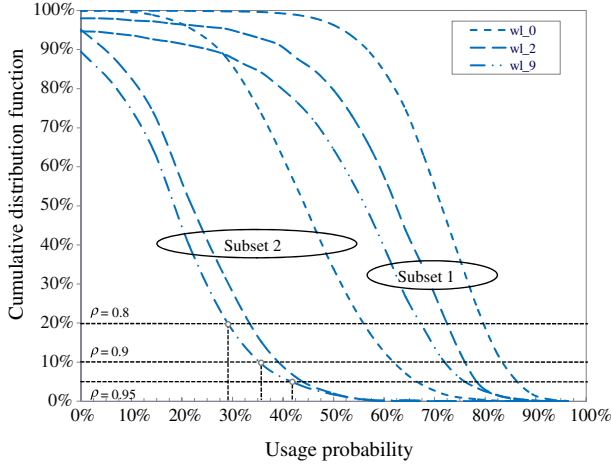


Fig. 2. (Color online) Cumulative distribution function of usage probability for three wavelength channels in links of subsets 1 and 2. Accuracy levels of 0.8, 0.9, and 0.95 are also shown.

Furthermore, we defined an accuracy level ( $\rho$ ) by undersizing the usage probability and assuming some small error. As shown in Fig. 2, three accuracy levels are considered (0.8, 0.9, and 0.95), thus obtaining different usage probabilities. For instance, wavelength channel #9 is in use with a probability of  $\sim 0.29$ ,  $\sim 0.35$ , and  $\sim 0.41$  on links in subset 2 assuming  $\rho$  equal to 0.8, 0.9, and 0.95, respectively.

As the final result of this stage, the usage probability ( $p_i(e)$ ) of each wavelength channel  $i$  on the links in the defined subsets is obtained. These values will be used to compute a probabilistic  $Q$ -factor of each of the lightpaths to be established over the network.

### B. In Operation: Probabilistic $Q$ -factor

With SAFIR, a probabilistic version of the  $Q$ -factor defined in Eq. (1) is computed for each candidate route. Following the approximated PLI model defined in Section II,  $pen_{eye}$ ,  $pen_{PMD}$ ,  $\sigma_{ASE}^2$ , and  $\sigma_{FWM}^2$  are pre-computed and stored at each controller node in the control plane. A set of values of  $pen_{eye}$  covering a specific range of lightpath distance are also pre-computed. On the other hand, the XPM noise variance for a given wavelength channel on a specific link is calculated by using the model presented in Eq. (4). Note that Eq. (3) cannot directly be applied in the context of SAFIR since the  $Q$ -factor of already-established lightpaths is not re-computed. Furthermore, although the usage status of every wavelength channel is flooded in the network, making it possible to calculate the current  $Q$ -factor, the value obtained might be immediately outdated as a consequence of the network dynamics. For these reasons, the deterministic  $\delta_i(e)$  in Eq. (3) is substituted by the usage probability ( $p_i(e)$ ), and a probabilistic version of the restricted approximated approach described in Section II can be obtained as follows, where the  $\sigma_{XPM}^2(e, \lambda)$  value computed represents a probabilistic bound with a given accuracy level of the XPM noise variance that a lightpath would experience on link  $e$  under the expected traffic distribution and offered load.

TABLE I  
SAFIR'S PROBABILISTIC IA-RWA ALGORITHM

```

IN network, set of  $k\_routes$ ,  $Q\_threshold$ 
OUT route and wavelength
1: Route candidateRoute
2: initialize  $w \leftarrow 0$ ;  $bestQ \leftarrow 0$ 
3: for each route  $r_i$  in  $k\_routes$  do
4:   for each wavelength  $w_i$  in  $W$  do
5:     if  $w_i$  is end-to-end available in  $r_i$  then
6:        $thisQ \leftarrow$  compute prob.  $Q$ -factor(network,  $r_i, w_i$ )
7:       if ( $thisQ > bestQ$ ) then
8:          $candidateRoute \leftarrow r_i$ 
9:          $w \leftarrow w_i$ ;  $bestQ \leftarrow thisQ$ 
10: if no candidateRoute found then
11:   return no route, lack of resources
12: if  $bestQ < Q\_threshold$  then
13:   return no route,  $Q$  reasons
14: return candidateRoute in wavelength  $w$ 

```

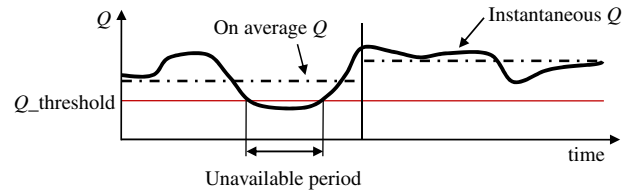


Fig. 3. (Color online) Evaluation of the  $Q$ -factor of an optical connection.

$$\sigma_{XPM}^2(e, \lambda) = \frac{\min(\lambda + \eta, |W|)}{\max_{i \neq \lambda}(1, \lambda - \eta)} p_i(e) \cdot s_{XPM}^2(e, \lambda, i). \quad (5)$$

Using the above probabilistic  $Q$ -factor, Table I presents the pseudo-code of an algorithm that selects a route, from a set of pre-computed routes for the source and destination nodes of a connection request, and assigns a wavelength so that its probabilistic  $Q$ -factor is better than a given threshold. For each candidate route, the algorithm computes the probabilistic  $Q$ -factor of every unused wavelength channel and chooses the lightpath with the maximum  $Q$  value. If no candidate route is found, the request is blocked due to insufficient resources. If the  $Q$ -factor of the lightpath found is lower than a given  $Q\_threshold$ , the connection request is blocked as a consequence of impairments constraints. Otherwise, the signaling of the connection request on the route found using the assigned wavelength starts. In the SAFIR approach, each source controller node runs this algorithm for every incoming connection request.

Although lightpaths are established only when their probabilistic  $Q$ -factor is above the threshold, there is no guarantee that a lightpath will not experience an XPM noise higher than the prediction. This in turn will lead to a lower  $Q$ -factor during part of its holding time (*instantaneousQ*). To quantify the insufficient  $Q$ -factor experienced by a lightpath, we propose to adopt the concept of availability. Similar to the availability defined in fault recovery [21], an optical connection becomes quality-of-transmission- (QoT-) unavailable when it experiences a BER higher than the requested threshold. Otherwise it remains QoT-available (Fig. 3). Connection QoT-availability (QoT-A) is defined as the ratio between the time

that a connection is QoT-available (i.e., satisfies the optical signal quality requirement) and the total time the connection is established in the network. Therefore, the inaccuracy of the decisions made by SAFIR can be quantified in terms of the QoT-unavailability (QoT- $U$ ) of the provisioned connections (or their complementary QoT-availability, QoT- $A = 1 - \text{QoT-}U$ ). Note, however, that even in the case of a lightpath experiencing QoT-unavailability, its *on-average*  $Q$  value, measured over a longer time period, might be above the required  $Q$  threshold, as shown in Fig. 3. In this regard, the *on-average*  $Q$  (BER) is the performance metric to be considered for service level agreements (SLAs) between network operators and customers.

*C. Changes in the Traffic Distribution: Re-characterization*

We assumed that a traffic distribution is forecasted in the network characterization phase. During network operation, traffic analysis must be done in order to determine the accuracy of traffic forecast. It is obvious that any characterization includes some error. Let us assume a standard confidence level of 95%. According to this assumption, some differences between the forecasted and the real traffic distribution may exist. In addition, the traffic distribution can change in the long term. Thus, a mechanism to trigger network re-characterization when the real traffic distribution moves to a new distribution (with a difference that is bigger than the confidence interval considered) must be devised. This adaptive mechanism is based on the monitoring of the traffic pattern to detect deviations with respect to the forecasted traffic distribution.

It is important to distinguish whether the deviations in the traffic distribution are within the confidence interval or not. In the latter case, a network re-characterization is triggered. The chi-squared test [19] can be used to this end.

IV. PERFORMANCE EVALUATION

This section evaluates the PLI model proposed in Section II. First, the networks considered are characterized to obtain the expected fiber usage values that will be applied by SAFIR. Then these networks are put into operation and the performance of SAFIR is evaluated in terms of blocking probability, QoT-availability, and setup time.

*A. PLI Model Validation*

Recall that our PLI model includes a statistical XPM model and assumes the worst case for FWM.

To minimize the XPM model’s error while keeping the size of the model at a moderate level, the value of parameters  $\eta$  and  $\gamma$  of the XPM model in Eqs. (3) and (4) need to be determined. We first studied the impact of  $\eta$  over both the number of polynomial models considered and the amount of information that the XPM model incorporates (i.e., the relative effect of  $2 * \eta$  neighbor channels over the XPM variance for a given

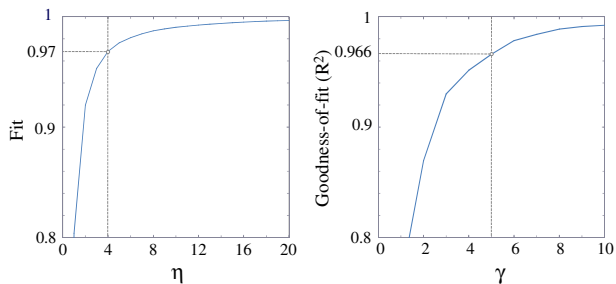


Fig. 4. (Color online) Selection of  $\eta$  and  $\gamma$  values. Fit of  $\sigma_{\text{XPM}}^2(e, \lambda)$  against  $\eta$  (left) and goodness of fit of the XPM model against  $\gamma(\eta = 4)$  (right).

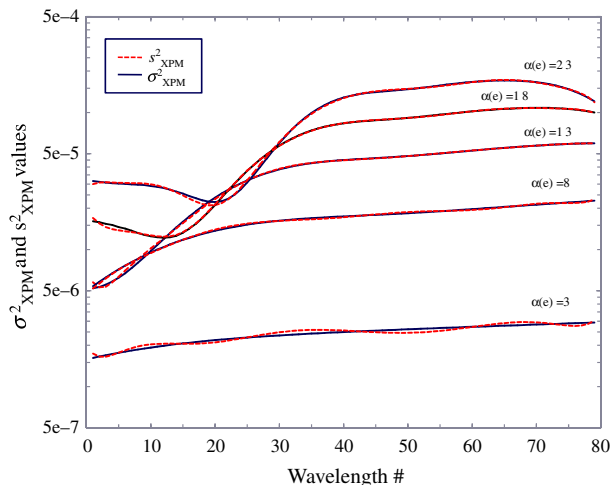


Fig. 5. (Color online) Analytical-to-statistical comparison for  $i = \lambda + 1$ .

reference channel). Using Eq. (3), the amount of information in  $\sigma_{\text{XPM}}^2(e, \lambda)$  against  $\eta$  is plotted in Fig. 4. The figure shows that  $\eta = 4$  adds about 97% of the total XPM effect, which, as will be proved, is enough for the model. Next, we used this value in our XPM statistical model and we applied a polynomial fitting [19] over a set of data which included 80 wavelengths for each of the  $2 * \eta s_{\text{XPM}}^2(e, \lambda, i)$  models. Several  $\gamma$ -degree polynomials were fitted, and the level of accuracy in terms of the Pearson correlation coefficient ( $R^2$ ) [19] is plotted in Fig. 4. As shown, 5-degree polynomials can be used while providing  $R^2$  values  $\geq 96\%$ .

Using these values for  $\eta$  and  $\gamma$ , our restricted approximated XPM model was compared against the analytical model in [16]. The solid lines in Fig. 5 present  $\sigma_{\text{XPM}}^2(e, \lambda, i)$  values for  $i = \lambda + 1$  of the links, with  $\alpha(e)$  ranging from 3 to 23 and with  $\lambda = 1 \dots 79$ . The dotted lines show  $s_{\text{XPM}}^2(e, \lambda, i)$  values for the same range of values of  $\alpha(e)$  and  $\lambda$  as before. It can be clearly seen that the values of XPM variance obtained by using our proposed statistical model are very close to that derived from the analytical model. The error introduced by the statistical model is shown as a function of the value of  $\sigma_{\text{XPM}}^2$  in Fig. 6. The vast majority of  $\sigma_{\text{XPM}}^2$  values are obtained with an error lower than  $\pm 5\%$ , but a few of them are computed with higher error. However, most of these higher error values correspond to a low  $\sigma_{\text{XPM}}^2$  value that adds a low or negligible total error to the final  $Q$ -factor value of a lightpath, as will be proved

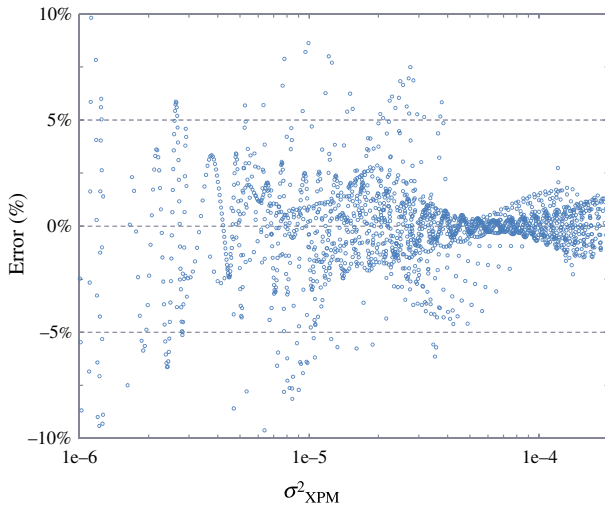


Fig. 6. (Color online) Analytical-to-statistical error as a function of  $\sigma_{\text{XPM}}^2(e, \lambda, i)$  for  $\eta = 4$  and  $\gamma = 5$ .

next. Interestingly, for higher  $\sigma_{\text{XPM}}^2$  values the error is within  $\pm 2.5\%$ . In addition to these results, a final validation of the statistical model applied to end-to-end lightpath provisioning is performed and presented later in this section.

Regarding the size of the XPM model, Table II shows the number of coefficients that need to be stored for the different XPM models in the case of fiber links with up to 25 amplifiers (i.e., up to 2000 km) using 40 or 80 wavelengths. It is worth noting that the number of coefficients to be stored is only 288 in the case of our restricted approximated model. In addition, note that the number of coefficients in the proposed model is not even dependent on the number of wavelengths considered.

The size of the complete PLI model, however, is slightly larger, since all other impairments are also pre-computed and stored. The number of  $pen_{\text{eye}}$  values to be stored depends on the assumptions for the values of the longest distance possible for a path and for the distance granularity. In our approach, a longest distance of 10,000 km and a distance granularity of 25 km are assumed, and thus 400  $pen_{\text{eye}}$  values are stored at each controller node. Moreover,  $|E|$  values for  $pen_{\text{PMD}}$ ,  $|E|$  for  $\sigma_{\text{ASE}}^2$ , and  $|E| * |W|$  values for the worst-case  $\sigma_{\text{FWM}}^2$  are also stored. In case of a network with 20 optical links and 80 wavelengths, our approach requires storing at each controller node in the control plane only 2328 PLI values, including the XPM variance.

Although the statistical XPM model has proved to provide low relative error (only 6%) when computing the XPM variance of a given link, it should also be validated to compute the

TABLE II

NUMBER OF COEFFICIENTS AND RELATIVE ERROR OF EACH MODEL

	$ W  = 40$	$ W  = 80$	Relative error ( $\epsilon_{\text{link}}$ )
Full deterministic	39,000	158,000	0%
Restricted ( $\eta = 4$ )	8000	16,000	3%
Restricted approximated ( $\eta = 4$ $\gamma = 5$ )		288	6%

Q-factor of lightpaths, specifically when a decision needs to be taken to accept or block a lightpath. To this end, and for the rest of our experiments, we used three network topologies: (i) the 16-node basic topology of the EON-BT [22], (ii) the 28-node ring topology of the European optical network (EON-RT) [22], and (iii) the 17-node NSF east network topology (NSF-East) [23]. These three network topologies were selected by considering their different average nodal degree and link length. Figure 7 shows the topologies considered and reviews their most relevant characteristics. Moreover, we assumed  $Q_{\text{threshold}} = 6$  ( $\text{BER} \approx 1e-9$ ).

The proposed PLI model is validated using the network topologies considered. We run several simulations for two values of offered network load, i.e., low and high, and the RWA decisions made by an exact analytical model [1] and our approximated impairments model are compared. Table III shows that the proposed PLI model makes incorrect decisions only in less than 0.11% of all cases. These results ensure that our model is responsible only for a negligible increment in the blocking probability.

## B. Network Characterization

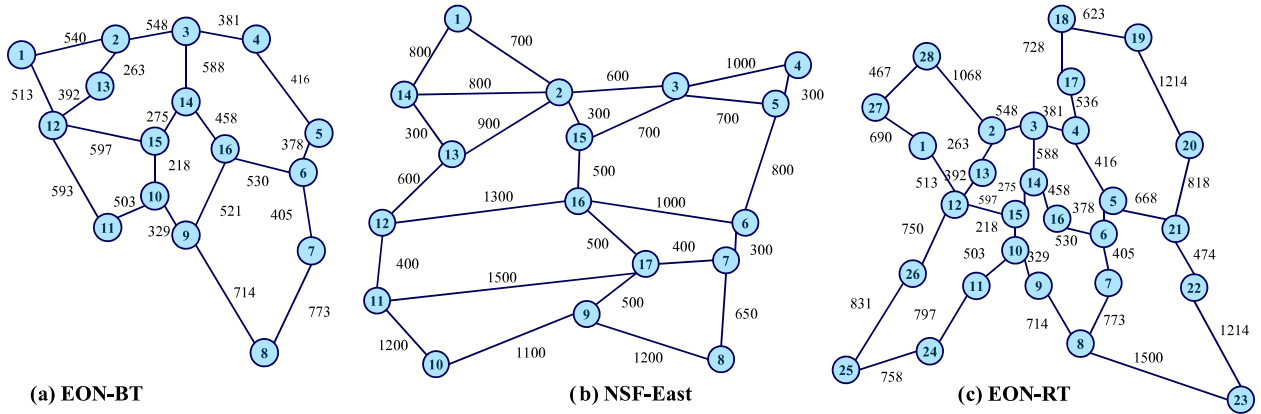
As described in Section III, before putting SAFIR into operation, an *on-average* usage distribution of each wavelength channel for a given traffic distribution and intensity should be obtained. To achieve this, we developed an ad hoc event-driven simulator in Matlab [24]. A dynamic network environment was simulated for the networks under study, in which incoming connection requests arrive at the system following a Poisson process and are sequentially served without prior knowledge of future incoming connection requests. The holding time of the connection requests is exponentially distributed with a mean value equal to 2 h. Source/destination pairs are randomly chosen with equal probability (uniform distribution) among all network nodes. Different values of the offered network load are created by changing the arrival rate while keeping the mean holding time constant. Furthermore, it is assumed that the bandwidth demand of each connection request is equal to one wavelength unit and that wavelength conversion capability is not available, i.e., the wavelength continuity constraint is enforced.

Figure 8 shows an example of the values obtained for  $p_i(e)$  on a link  $e$  with a maximum capacity of 40 wavelengths for the accuracy levels considered using  $\eta = 4$  and  $\gamma = 5$ . It can be noticed that  $\eta$  affects the usage probability of the wavelength channels, since a clear distribution for the  $p_i(e)$  values can be identified. For instance, wavelength channels #0 and #39 have significantly higher usage probability as compared to channels #1...# $\eta$  and #(39 -  $\eta$ )...#38.

## C. SAFIR Performance Evaluation

The performance of SAFIR was compared against two benchmarking impairment-aware strategies, i.e., a *distributed* approach and a *worst-case* approach.

The distributed approach, referred to as the *impairment-aware current state (IA-CS)*, computes the Q-factor of each



Network	Nodes	Links	Nodal degree	Min. Length	Aver. Length	Max. Length
EON-BT	16	21	2.63	218	473	597
NSF-East	17	26	3.06	300	630	1500
EON-RT	28	34	2.43	218	733	1500

Fig. 7. (Color online) Network topologies considered: (a) 16-node EON-BT [22], (b) 17-node NSF-East [23], and (c) 28-node EON-RT [22].

TABLE III  
PLI MODEL FINAL VALIDATION ( $Q$  DECISIONS)

	EON-BT		EON-RT		NSF-East	
<b>Load (Erlangs)</b>	<b>270</b>	<b>330</b>	<b>210</b>	<b>300</b>	<b>270</b>	<b>360</b>
<b>Decisions</b>	10,027	9936	10,010	10,000	10,035	10,020
<b>Wrong</b>	0	1	0	1	0	11
<b>%</b>	0	0.01	0	0.01	0	0.11

candidate lightpath using the current state of the network. For this reason *IA-CS* requires accurate and complete knowledge of the network resource usage. *IA-CS* works as follows. If the  $Q$ -factor of a candidate lightpath is lower than  $Q_{\text{threshold}}$ , the connection request is rejected; if the  $Q$ -factor is higher than  $Q_{\text{threshold}}$ , *IA-CS* makes sure that this candidate lightpath will not affect the already-established connections by re-computing the  $Q$ -factor of the existing lightpaths that share fiber links with the new lightpath. If the  $Q$ -factor of every already-established lightpath is higher than the threshold, the new lightpath is established; otherwise, the connection request is blocked.

The worst-case approach, referred to as the *Impairment-aware Worst Case (IA-WC)*, assumes that all wavelengths are in use on every link of the network, and hence the  $Q$ -factor is not dependent on the load of the links. With this strategy, the information about the current network state is not needed and the  $Q$ -factor re-computation of already-established lightpaths is not necessary.

Ad hoc event-driven simulators for all approaches considered were implemented in Matlab. The number of shorter routes ( $k$ ) was fixed to 10 for all cases. We conducted a number of simulations using the previously described uniform traffic distribution. For all the blocking probability results, the simulation time was set to achieve a confidence interval of 5% or better, with 95% confidence level.

Figure 9 shows the total blocking probability accounting for both blocking due to insufficient resources, i.e., when no

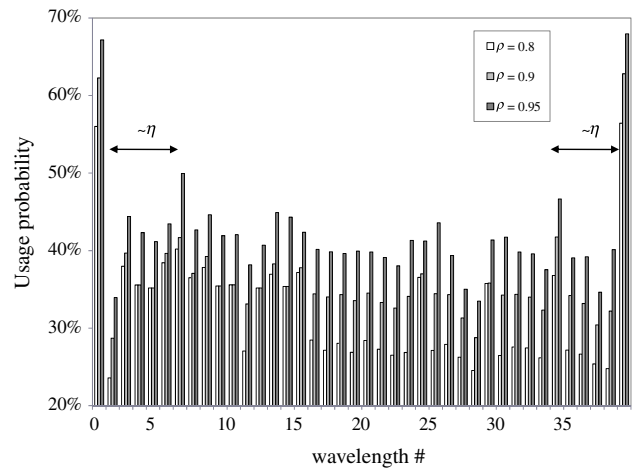


Fig. 8. Usage probability of each wavelength in a link ( $|W| = 40$ ) for accuracy levels of 0.8, 0.9, and 0.95, using  $\eta = 4$  and  $\gamma = 5$ .

wavelength is available, and due to impairment constraints, i.e., when none of the candidate lightpaths can meet  $Q_{\text{threshold}}$ . To find the lower bound on the total blocking probability we applied a conventional shortest path routing approach with FF wavelength assignment, referred to as *NoIA-RWA*, i.e., a connection request is blocked due to insufficient resources only. Different values of the offered network load are considered in each network topology tested

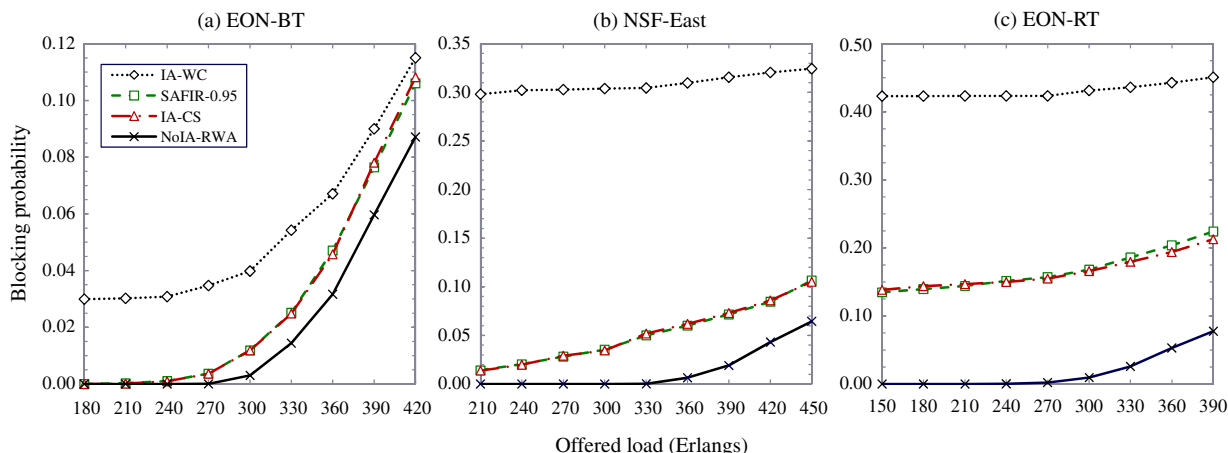


Fig. 9. (Color online) Blocking probability versus the offered network load.

by selecting the values where the blocking probability obtained by NoIA-RWA does not exceed 8%. As expected, IA-WC exhibits the worst blocking probability performance in all topologies tested. This is because IA-WC calculates the  $Q$ -factor of a lightpath by assuming that all wavelengths are in use. On the other hand, the results show that SAFIR with  $\rho = 0.95$  has similar blocking results to IA-CS without requiring any information about the current network state or extra calculations to check the  $Q$ -factor value of previously established lightpaths. Note that the blocking probability obtained by all approaches tested in the case of EON-RT is as high as 13% even for low offered network load. This is because the high average link length leads to high blocking due to impairment constraints.

Both IA-WC and IA-CS guarantee that, for the entire connection holding time, all established lightpaths will have a  $Q$ -factor value better than or equal to  $Q_{\text{threshold}}$ . However, as explained in Section III, this is not true for SAFIR. In order to quantify the effect of using network characterization rather than the current network state in SAFIR, three different accuracy levels of wavelength usage probability, i.e.,  $\rho = 0.8$ ,  $\rho = 0.9$ , and  $\rho = 0.95$ , are tested for the selected loads. The blocking probability ( $P_b$ ) and the QoT- $U$  values are shown in Table IV for three levels of the load and accuracy of the wavelength usage. The results show that the average QoT-unavailability obtained using SAFIR is around  $1e-4$  in EON-BT and EON-RT and around  $1e-3$  in NSF-East. This is a consequence of longer distances in the latter. It should be mentioned that QoT- $U = 1e-3$  entails lightpaths experiencing a lower  $Q$  (worse BER) than the threshold during only 0.1% of time. The highest observed *instantaneous* BER for the lightpaths was equal to  $2.3e-8$ , which is only slightly above the considered BER threshold of  $1e-9$ . However, *on-average* BER values of lightpaths for time periods of 1 h show that, even when the instantaneous BER value is under the threshold, the 1 h *on-average* BER values were never worse than  $3.84e-10$ , which clearly proves how SAFIR fulfills SLA agreements.

As expected, QoT- $U$  values increase when the accuracy level is reduced. This is because the channel usage is underestimated, so the values of the probabilities are lower and in turn the blocking probability is higher.

Next, we study how SAFIR deals with (small) changes in the forecasted traffic distribution as a consequence of errors in its characterization. To this end, we add some traffic following the stringent dual-hub distribution [21], in which every node in the network connects to only two destination nodes, known as hubs. The real traffic distribution is then in the form  $\alpha * \text{uniform} + (1 - \alpha) * \text{dual-hub}$ . Note that, in this case, the incoming links to the hub nodes would be much more loaded compared to the expected usage values obtained during the initial characterization phase.

Table V reproduces the results obtained for the EON-BT (Fig. 7(a)) network assuming 5% ( $\alpha = 95\%$ ) and 10% ( $\alpha = 90\%$ ) of traffic following the dual-hub distribution, in which nodes 15 and 16 are selected as the hub nodes. As shown, SAFIR offers almost the same  $P_b$  values as the ones achieved by the IA-CS scheme under low and medium loads. Although under the highest load the value of  $P_b$  obtained by SAFIR is perceptibly different from that of IA-CS, it is worth noting that these load levels are far from the optimum operational load (i.e., at which  $P_b \leq 1\%$ ) commonly used in real network scenarios. On the other hand, in all the loads considered the QoT- $U$  value obtained is very low.

Additionally, we perform the chi-squared test to randomly sample the connection requests following the mix of the uniform and the dual-hub distributions with  $\alpha = 95\%$  and compare them against the pure uniform one. Note that if the size of the sample (the number of connection requests monitored) is very high, we could detect any small difference between samples generated following two different distributions, even in the case of very small deviation in the distributions. However, large sample sizes entail long monitoring times; thus the key point is to detect deviations as soon as they appear. We find that we need to monitor of the order of 4000 requests to detect deviations in the forecasted traffic distribution. In the case of the EON-BT network under a traffic load resulting in  $P_b = 1\%$  (330 Erlangs), by assuming a mean holding time of 2 h, the mean inter-arrival time is as stringent as 22 s. As a consequence, even in the stringent scenario described above, we need to monitor the network every day and decide whether or not re-characterization is needed.

TABLE IV  
BLOCKING PROBABILITY AND QoT-UNAVAILABILITY OF LIGHTPATHS USING SAFIR FOR DIFFERENT ACCURACY LEVELS

Network	$\rho$	Low Load		Medium Load		High Load	
		$P_b$	QoT-U	$P_b$	QoT-U	$P_b$	QoT-U
EON-BT	0.95	0%	0	1.19%	1.20e-5	10.60%	1.03e-4
	0.9	0%	0	1.18%	2.38e-5	10.55%	1.27e-4
	0.8	0%	0	1.13%	2.76e-5	10.33%	1.64e-4
NSF-East	0.95	1.43%	1.26e-3	5.00%	1.86e-3	10.64%	2.44e-3
	0.9	1.40%	1.31e-3	4.44%	1.85e-3	10.33%	2.68e-3
	0.8	1.03%	1.57e-3	4.36%	1.96e-3	10.32%	2.78e-3
EON-RT	0.95	13.49%	1.62e-5	15.69%	1.85e-4	22.41%	1.82e-6
	0.9	12.85%	1.63e-5	14.73%	2.04e-4	21.42%	1.85e-5
	0.8	12.09%	1.87e-5	13.63%	2.57e-4	20.36%	2.04e-5

TABLE V  
 $P_b$  AND QoT-U CONSIDERING TRAFFIC DISTRIBUTION DEVIATIONS

Dual-hub traffic	Approach	Low Load		Medium Load		High Load	
		$P_b$	QoT-U	$P_b$	QoT-U	$P_b$	QoT-U
5%	SAFIR	0	0	1.2%	0	9.8%	0
	IA-CS	0	0	1.3%	0	12.7%	0
10%	SAFIR	0	0	1.6%	7.7e-6	9.9%	7.4e-5
	IA-CS	0	0	1.5%	0	12.8%	0

TABLE VI  
MEAN TIMES CONSIDERED

$t_{RWA}$	20 ms	$t_{OCC}$	0.5 ms
$t_{link}$	0.25 ms	$t_{switch}$	5 ms
	+propagation time	$t_{config}$	2 ms

As mentioned in the introduction, the  $Q$ -factor computation time strongly impacts the lightpath setup times when an IA-CS strategy is used. In order to better assess the advantages of SAFIR, we quantified the lightpath setup times ( $t_{setup}$ ) using an equation similar to the one presented in [25], but adding the  $Q$ -factor computation time to consider a PLI-aware environment.  $t_{setup}$  can be computed as

$$t_{setup} = t_{RWA} + (2n - 1) \cdot t_{OCC} + 2 \cdot (n - 1) \cdot t_{link} + t_{config} + t_{switch} + q \cdot t_Q, \quad (6)$$

where  $t_{RWA}$  represents the computation time of the RWA algorithm (excluding the  $Q$ -factor computation),  $t_Q$  is the  $Q$ -factor computation time,  $t_{OCC}$  is the processing time in each controller in the control plane,  $t_{link}$  is the propagation delay in each control network link,  $t_{config}$  is the software configuration time of an optical node,  $t_{switch}$  is the time to perform the optical switching,  $n$  represents the number of nodes traversed by the lightpath, and  $q$  is the number of  $Q$ -factor computations. Note that  $q$  includes both the number of  $Q$ -factor computations performed during the wavelength assignment process of a new lightpath and the number of computations needed to check already-established lightpaths, which could be calculated in parallel. Table VI specifies the values used for the parameters, which are in line with those in [25].

Two general strategies for the wavelength assignment process were considered to compare the setup times: (i) first fit (WA-FF), in which the first end-to-end available wavelength

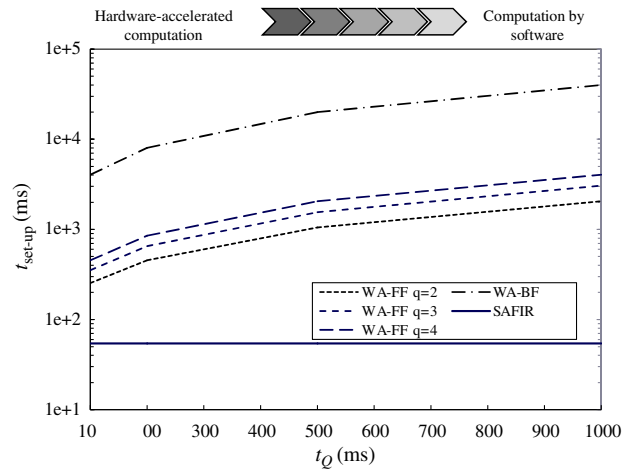


Fig. 10. (Color online) Lightpath setup time as a function of  $Q$ -factor computation time using the standard IA-CS strategy. The performance of the SAFIR approach is shown for comparison.

with a  $Q$  value higher than the threshold is selected, thus minimizing the number of  $Q$ -factor computations, and (ii) best fit (WA-BF), in which the wavelength with the best  $Q$  value is selected after computing the  $Q$ -factor of every end-to-end available wavelength. A  $Q$ -factor computation time of the order of 100 ms can be obtained using specific dedicated hardware, whereas the time to compute the  $Q$ -factor without special hardware is in the order of seconds [10,17].

Figure 10 plots the lightpath setup time as a function of the time needed to compute the  $Q$ -factor using the IA-CS strategy with both WA-FF and WA-BF. The route of all lightpaths considered consisted of four nodes ( $n = 4$ ) with 600 km fiber links. For comparison purposes, the setup times achieved by SAFIR are also plotted assuming  $q = 1$  and  $t_Q = 10$  ms. The

figure shows that a setup time shorter than 100 ms can be achieved by using SAFIR while a setup time of one or of several seconds is needed using the IA-CS strategy. It is worth noting that even by using the WA-FF heuristic at least two  $Q$ -factor computations can be expected, one to assign the wavelength and then, once the  $Q$ -threshold is checked, another for the already-established lightpaths.

## V. CONCLUSIONS

In this paper, a PLI model for fast  $Q$ -factor computation in optical transparent WDM networks was proposed. This model includes a statistical estimation of XPM. The accuracy of the model was validated via simulations. It was shown that our statistical model obtains the XPM noise variance with maximum 6% error when compared to the values offered by an analytical model. Moreover, the PLI model made a correct lightpath selection in 99.89% of all the cases, compared to an exact analytical impairments model.

Based on the advantages of our PLI model, a novel statistics-based approach for fast impairment-aware RWA, referred to as SAFIR, was proposed. SAFIR uses network characterization combined with the validated PLI model to compute a probabilistic version of the lightpath  $Q$ -factor. In this way the information about the current network state is not needed, implying no extension of GMPLS. In light of the results obtained, the total blocking probability achieved by SAFIR was very close to the one computed via a distributed approach in all network topologies tested for different accuracy levels of wavelength channel usage probability.

Since the statistical values for channel usage in each link may affect the quality of the lightpaths provisioned by SAFIR, the  $Q_oT-U$  concept related to excessive BER was introduced to evaluate the inaccuracy of the proposed approach. In the entire set of the performed tests, the  $Q_oT-U$  of all established lightpaths was kept below  $1e-3$ . Even for that  $Q_oT-U$  value, the 1 h *on-average* BER values were always above the threshold.

Finally, lightpath setup times achieved by SAFIR were compared against those using the IA-CS strategy in distributed environments. As proved, SAFIR offers setup times shorter than 100 ms instead of several seconds obtained by the IA-CS strategy together with hardware-accelerated  $Q$ -factor computation.

In conclusion, SAFIR removes the prohibitively high control overhead of the IA distributed approaches while providing comparable network performance.

## ACKNOWLEDGMENTS

A preliminary version of this paper was presented at the OFC Conference in 2010. The work presented in this paper was supported by the Network of Excellence "Building the Future Optical Network in Europe" (BONE), funded by the European Commission through the 7th ICT-Framework Programme, and by the Spanish science ministry through the TEC2011-27310 ELASTIC project.

## REFERENCES

- [1] A. Jirattigalachote, P. Monti, L. Wosinska, K. Katrinis, and A. Tzanakaki, "ICBR-Diff: an impairment constraint based routing strategy with quality of signal differentiation," *J. Networks*, vol. 5, pp. 1279–1289, 2010.
- [2] P. Pavon-Marino, S. Azodolmolky, R. Aparicio-Pardo, B. Garcia-Manrubia, Y. Pointurier, M. Angelou, J. Sole-Pareta, J. Garcia-Haro, and I. Tomkos, "Offline impairment aware RWA algorithms for cross-layer planning of optical networks," *J. Lightwave Technol.*, vol. 27, pp. 1763–1775, 2009.
- [3] R. Martinez, C. Pinart, F. Cugini, N. Andriolli, L. Valcarenghi, P. Castoldi, L. Wosinska, J. Comellas, and G. Junyent, "Challenges and requirements for introducing impairment-awareness into the management and control planes of ASON/GMPLS WDM networks," *IEEE Commun. Mag.*, vol. 44, no. 12, pp. 76–85, 2006.
- [4] F. Agraz, S. Azodolmolky, M. Angelou, J. Perelló, L. Velasco, S. Spadaro, A. Francescon, C. V. Saradhi, Y. Pointurier, P. Kokkinos, E. Varvarigos, M. Gunkel, and I. Tomkos, "Experimental demonstration of centralized and distributed impairment-aware control plane schemes for dynamic transparent optical networks," in *Optical Fiber Communication Conf. (OFC)*, 2010, PDPD5.
- [5] S. Azodolmolky, M. Klinkowski, E. Marín, D. Careglio, J. Solé-Pareta, and I. Tomkos, "A survey on physical layer impairments aware routing and wavelength assignment algorithms in optical networks," *Comput. Netw.*, vol. 53, pp. 926–944, 2009.
- [6] R. Cardillo, V. Curri, and M. Mellia, "Considering transmission impairments in wavelength routed networks," in *Conf. on Optical Networking Design and Modeling (ONDM)*, 2005, pp. 421–429.
- [7] D. Monoyios and K. Vlachos, "Multiobjective genetic algorithms for solving the impairment-aware routing and wavelength assignment problem," *J. Opt. Commun. Netw.*, vol. 3, pp. 40–47, 2011.
- [8] S. Pachnicke, T. Paschenda, and P. Krummrich, "Assessment of a constraint-based routing algorithm for translucent 10 Gbits/s DWDM networks considering fiber non-linearities," *J. Opt. Netw.*, vol. 7, pp. 365–377, 2008.
- [9] E. Salvadori, Y. Yabin, C. Saradhi, A. Zanardi, H. Woesner, M. Carcagni, G. Galimberti, G. Martinelli, A. Tanzi, and D. La Fauci, "Distributed optical control plane architectures for handling transmission impairments in transparent optical networks," *J. Lightwave Technol.*, vol. 27, pp. 2224–2239, 2009.
- [10] S. Azodolmolky, J. Perelló, M. Angelou, F. Agraz, L. Velasco, S. Spadaro, Y. Pointurier, A. Francescon, C. Vijaya, P. Kokkinos, E. Varvarigos, S. Al Zahr, M. Gagnaire, M. Gunkel, D. Klondis, and I. Tomkos, "Experimental demonstration of an impairment aware network planning and operation tool for transparent/translucent optical networks," *J. Lightwave Technol.*, vol. 29, pp. 439–448, 2011.
- [11] "Architecture for the automatically switched optical network (ASON)," *ITU Recommendation G.8080/Y.1304*, Nov. 2001.
- [12] E. Mannie, "Generalized multi-protocol label switching (GMPLS) architecture," *IETF RFC-3945*, 2004.
- [13] S. Ten, K. Ennsner, J. Grochocinski, S. Burtsev, and V. daSilva, "Comparison of four-wave mixing and cross phase modulation penalties in dense WDM systems," in *Optical Fiber Communication Conf. (OFC)*, 1999, pp. 43–45.
- [14] R. Hui, K. Demarest, and C. Allen, "Cross-phase modulation in multispan WDM optical fiber systems," *J. Lightwave Technol.*, vol. 17, pp. 1018–1026, 1999.
- [15] A. Cartaxo, "Cross-phase modulation in intensity modulation-direct detection WDM systems with multiple optical amplifiers

- and dispersion compensators," *J. Lightwave Technol.*, vol. 17, pp. 178–190, 1999.
- [16] S. Pachnicke and E. Voges, "Analytical assessment of the  $Q$ -factor due to cross-phase modulation (XPM) in multispan WDM transmission systems," *Proc. SPIE*, vol. 5247, pp. 61–70, 2003.
- [17] Y. Qin, S. Azodolmolky, M. Gunkel, R. Nejabati, and D. Simeonidou, "Hardware accelerated impairment-aware control plane for future optical networks," *IEEE Commun. Lett.*, vol. 15, pp. 1004–1006, 2011.
- [18] N. Sambo, M. Secondini, F. Cugini, G. Bottari, P. Iovanna, F. Cavaliere, and P. Castoldi, "Modeling and distributed provisioning in 10–40–100-Gb/s multirate wavelength switched optical networks," *J. Lightwave Technol.*, vol. 29, pp. 1248–1257, 2011.
- [19] D. Montgomery, *Design and Analysis of Experiments*. Wiley & Sons, 2004.
- [20] D. Leung and W. Grover, "Capacity planning of survivable mesh-based transport networks under demand uncertainty," *Photonic Network Commun.*, vol. 10, pp. 123–140, 2005.
- [21] W. Grover, *Mesh-Based Survivable Transport Networks: Options and Strategies for Optical, MPLS, SONET and ATM Networking*. Prentice Hall, 2003.
- [22] S. Maeschalck, D. Colle, I. Lievens, M. Pickavet, P. Demeester, C. Mauz, M. Jaeger, R. Inkret, B. Mikac, and J. Derkacz, "Pan-European optical transport networks: An availability-based comparison," *Photonic Network Commun.*, vol. 5, pp. 203–225, 2003.
- [23] L. Song and B. Mukherjee, "Accumulated-downtime-oriented restoration strategy with service differentiation in survivable WDM mesh networks," *J. Opt. Commun. Netw.*, vol. 1, pp. 113–124, 2009.
- [24] MATLAB [Online]. Available: <http://www.mathworks.com/products/matlab/>.
- [25] L. Velasco, F. Agraz, R. Martínez, R. Casellas, S. Spadaro, R. Muñoz, and G. Junyent, "GMPLS-based multi-domain restoration: Analysis, strategies, policies and experimental assessment," *J. Opt. Commun. Netw.*, vol. 2, pp. 427–441, 2010.